Dynamics and Multi-configuration Potential Energy Surface for the Singlet O_2 Reactions with Radical Cations of Guanine, 9-Methylguanine, 2′-Deoxyguanosine and Guanosine

Yan Sun,[ab] Midas Tsai,[c] May Myat Moe,[ab] and Jianbo Liu*[ab]
[a] Department of Chemistry and Biochemistry, Queens College of the City University of New York, 65-30 Kissena Blvd., Queens, NY 11367, USA; [b] Ph.D. Program in Chemistry, The Graduate Center of the City University of New York, 365 5th Ave., New York, NY 10016, USA; [c] Department of Natural Sciences, LaGuardia Community College 31-10 Thomson Ave., Long Island City, NY 11101, USA

Abstract Reactions of electronically excited singlet oxygen ($^1O_2$) with the radical cations of guanine ($9HG^{\bullet+}$), 9-methylguanine ($9MG^{\bullet+}$), 2′-deoxyguanosine ($dGuo^{\bullet+}$) and guanosine ($Guo^{\bullet+}$) were studied in the gas phase by a combination of guided-ion-beam mass spectrometric measurement of product ions and cross sections as a function of collision energy (E_{col}) and electronic structure calculations of reaction potential energy surface (PES) at various levels of theory. No product could be captured in the $^1O_2$ reaction with bare $9HG^{\bullet+}$ or $9MG^{\bullet+}$, because energized products decayed rapidly to reactants before being detected. To overcome this unfavorable kinetics, monohydrated $9HG^{\bullet+}\cdot H_2O$ and $9MG^{\bullet+}\cdot H_2O$ were used as reactant ions, of which the peroxide product ions were stabilized by energy relaxation via elimination of the water ligand. Reaction cross sections for $9HG^{\bullet+}\cdot H_2O$ and $9MG^{\bullet+}\cdot H_2O$ decrease with increasing E_{col}, becoming negligible above 0.6 eV. This indicates that the reactions are exothermic with no barriers above reactants and the heat of formation of the products is sufficiently large to overcome their water ligand elimination energy (0.7 eV). Peroxide product ions were also detected in the $^1O_2$ reactions with unhydrated $dGuo^{\bullet+}$ and $Guo^{\bullet+}$, in which intramolecular vibrational redistribution was able to stabilize oxidation products. $9MG^{\bullet+}$ was utilized as a model system to explore reaction PES for the initial $^1O_2$ addition to guanine radical cation. Calculations were carried out using single-reference ωB97XD, RI-MP2 and DLPNO-CCSD(T) and multi-reference CASSCF and CASPT2. Despite the same PES profile was obtained at different levels of theory, the energies of the mixed open- and closed-shell $^1O_2$ reactant and the open-shell reaction intermediates, transition states and products are sensitive to the theories. By taking into account both static and dynamic electron correlations, the CASPT2 PES has provided the best agreement with the experimentally measured reaction thermodynamics and predicted 8-peroxide as the most probable initial oxidation product of guanine radical cation.

---

* E-mail: jianbo.liu@qc.cuny.edu. Tel: 1-718-997-3271.

1. Introduction

Compared to the adenine (A), cytosine (C) and thymine (T) nucleobases, guanine (G) has the lowest oxidation potential ($E°$ *vs.* NHE = 1.29 V for guanosine, 1.42 V for adenosine, 1.6 V for deoxycytidine and 1.7 V for thymidine)[1-2] and the lowest adiabatic ionization energy (AIE = 7.75 eV for G, 8.27 eV for A, 8.66 eV for C and 8.82 eV for T).[3-4] This makes guanine the primary target for one-electron oxidation, leading to the facile formation of guanine radical cation ($G^{\bullet+}$) upon radiolysis,[5-6] photolysis,[7] chemical oxidation,[8] electron transfer between DNA-bound metal complexes,[9] electrocatalytic oxidation[10-11] and type I photosensitized oxidation.[12-13] The complementary base pairing of G with C in double helical DNA further reduces its $E°$ by 0.28 – 0.34 V[14-15] and AIE by 0.75 – 0.78 eV.[16-17] In line with these facts, electron holes that are initially created by one-electron oxidation of other nucleobases may migrate for long distances from the locus of formation to the guanine sites,[18] rendering the formation of $G^{\bullet+}$ as an ultimate trap for the oxidative damage to DNA.[6] Formation of $G^{\bullet+}$ is the first step toward a variety of biological sequelae,[19-22] most of which are highly mutagenic, *e.g.*, 8-oxo-7,8-dihydroguanine (8-OG, the most common product produced in vivo under oxidative stress[23]) lesion[20] in genomic, mitochondrial and telomeric DNA.

Of relevance to the guanine-mediated DNA lesions is the electronically excited singlet oxygen ($O_2[a^1\Delta_g]$)-induced damage. $^1O_2$ is generated in living systems through enzymatic and nonenzymatic reactions, type II photosensitization, chemical excitation, etc.[24-25] and is known to cause DNA damage.[20, 26-29] The $^1O_2$ damage to DNA initiates exclusively at the guanine residues.[20-22, 26-48] The consequential primary and secondary damage is implicated in DNA strand breaks,[2] DNA-protein cross-links,[43, 48] mutation[49] and apoptosis[50] as well as in photodynamic therapy for cancer.[51] Most of the mechanistic insights on the $^1O_2$ oxidation of guanine were obtained from the measurements of guanine residues in various contexts (including isolated nucleobases, nucleosides, oligonucleotides, and single- and double-stranded DNA) in solution[26-40, 47-48] and their protonated and deprotonated ions in the gas phase,[44-46] augmented by reaction potential energy surface (PES) investigations[43-48, 52-53] and molecular dynamics simulations.[41-42, 44-46] A currently accepted mechanism is that guanine is attacked by $^1O_2$ on its imidazole ring, forming a transient peroxide and/or endoperoxide that quickly converts to a hydroperoxide 8-OOH-G. The 8-OOH-G in isolated nucleosides and short oligonucleotides undergoes a series of reactions and ultimately forms spiroiminodihydantoin and guanidinohydantoin;[35] whereas that within DNA is reduced to 8-OG.[28] A scenario of biological significance is ionizing radiation and/or one-electron oxidants interacting with DNA in the presence of $^1O_2$. Under that circumstance, synergistic effects from the combination of $G^{\bullet+}$ formation and $^1O_2$ oxidation are anticipated. Surprisingly, the reaction of $G^{\bullet+}$ with $^1O_2$ has not yet been directly measured or theoretically modeled. Neither of the reaction kinetics nor the nature of the oxidation products was known. On the other hand, the knowledge of such concurrent processes is not only of significance for the fundamental understanding of DNA oxidatively generated damage but also of high practical interest in exploring the additive effects of combing ionization radiation-based radiotherapy and $^1O_2$-based photodynamic therapy in cancer treatment.[54-56]

The degradation pathways of $G^{\bullet+}$ depend on structural context and reaction environments (*i.e.*, solvent and pH). In neutral aqueous solution, free $G^{\bullet+}$ (and that within single-stranded DNA) undergoes deprotonation through the loss of the imino proton at N1 to water and yields neutral radical $[G - H]^\bullet$ within 56 ns.[57-58] In contrast, $G^{\bullet+}$ within double-stranded DNA is stabilized through Watson-Crick base paring which diminishes the probability of deprotonation.[59] The fates of $G^{\bullet+}$ and $[G - H]^\bullet$ are distinctively different by following different transformations and producing different end products.[19-22] This implies that a direct measurement of $G^{\bullet+}$ with $^1O_2$ in aqueous solution is not feasible, because deprotonation of $G^{\bullet+}$ may be faster than oxidation and the oxidation behavior of deprotonated $[G - H]^\bullet$ may not faithfully mimic that of $G^{\bullet+}$ within DNA.[6] In this sense, a gas-phase environment is more appropriate for examining the $^1O_2$ oxidation of $G^{\bullet+}$ wherein deprotonation shuts down and reaction is not perturbed by solvent and counter ions. In the present work, the reactions of $^1O_2$ with the radical cations of guanine ($9HG^{\bullet+}$), 9-methylguanine ($9MG^{\bullet+}$), 2′-deoxyguanosine ($dGuo^{\bullet+}$) and guanosine ($Guo^{\bullet+}$) were investigated in the gas phase, in the order of increasing structural complexity. The guided-ion-beam scattering mass spectrometric measurement, combined with multi-configuration reaction PES modeling, constituted the first study on the chemistry of guanine radical cation with $^1O_2$.

2. Experimental and Theoretical Methods

2.1 Chemicals

9MG (Aldrich, >98.0%), dGuo (Sigma, >99%), Guo (Acros, 99%), $Cu(NO_3)_2$ (Alfa Aesar, 99.999%), KOH (Fisher Chemical, >85%) and aqueous H_2O_2 (Acros Organics, 35 wt%) were used without further purification. Chlorine gas (99.5%) was purchased from Sigma Aldrich, and helium gas (research grade) was purchased from T.W. Smith. All solvents were HPLC grade.

2.2 Generation and detection of $^1O_2$

$^1O_2$ was generated by the reaction of $H_2O_2 + Cl_2 + 2KOH \rightarrow {}^1O_2/{}^3O_2 + 2KCl + 2H_2O$.[60-61] In brief, 10.5 mL of 8 M KOH was added to 20 mL of 35 wt% aqueous H_2O_2 in a sparger held at -18 ºC. The mixture was degassed. 3.42 sccm of Cl_2 was mixed with 53.5 sccm of He in a gas proportioner and bubbled through the H_2O_2/KOH slush. Cl_2 reacted completely with H_2O_2 and produced a mixture of $^1O_2$, $^3O_2$ and water. Gas products passed through a cold trap (kept at -70 ºC) to remove water vapor. Only $^1O_2$, $^3O_2$ and He remained in the downstream gas. The concentration of $^1O_2$ was determined by measuring its $a^1\Delta_g \rightarrow X^3\Sigma_g^-$ emission[62] in an optical emission cell. Emission from the cell was collimated, passed through an optical chopper and filtered by a 5 nm-bandwidth interference filter centered at 1270 nm. The chopped emission was focused into a thermoelectrically cooled InGaAs photodetector (Newport 71887 detector and 77055 cooler) coupled with a lock-in amplifier (SRS model SR830). The amplifier output was converted to absolute $^1O_2$ concentration per a previous calibration.[63] To reduce wall- and self-quenching of $^1O_2$, the sparger was continuously evacuated and its pressure was maintained at 12.8 τ. At this pressure, a steady concentration of $^1O_2$ (up to 15%) was produced for conducting ion-molecule reactions.

2.3 Formation of guanine radical cation and ion-molecule scattering

Reaction of guanine radical cation with $^1O_2$ was carried out on a home-made electrospray ionization

(ESI) guided-ion-beam scattering tandem mass spectrometer at Queens College. Details of the apparatus can be found in our previous work.[64-65] As a source of guanine radical cations, we used collision-induced-dissociation (CID) of Cu(II)-nucleoside complexes.[65-67] A methanol/water (v:v = 3:1) solution of 0.25 mM $Cu(NO_3)_2$ and 0.5 mM guanosine was freshly prepared and sprayed into the air through an ESI needle at a rate of 0.06 mL/hr. The $[Cu^{II}(Guo)_{0\text{-}6}]^{\bullet 2+}\cdot(CH_3OH)_{0\text{-}3}$ complexes formed in the electrospray entered the source chamber of the mass spectrometer through a desolvation capillary which was biased at 115 V with respect to ground and heated up to 200 ºC. The source chamber was evacuated to a pressure of 1.7 τ. A 1.0 mm-orifice skimmer was located 3 mm away from the end of the desolvation capillary, separating the source chamber and a hexapole ion guide. The skimmer was biased at 17 V with respect to ground. The electrical field between the capillary and the skimmer prompted CID of $[Cu^{II}(Guo)_{0\text{-}6}]^{\bullet 2+}\cdot(CH_3OH)_{0\text{-}3}$ with the background gas in the source chamber, and the dissociation of $[Cu^{II}(Guo)_3]^{\bullet 2+}$ was featured by redox separation, *i.e.*, $[Cu^{II}(Guo)_3]^{\bullet 2+} \rightarrow [Cu(Guo)_2]^+ + Guo^{\bullet +}$. A fraction of $Guo^{\bullet +}$ ions eliminated the sugar group ($-C_5H_8O_4$) in CID and produced $9HG^{\bullet +}$. Likewise, $9MG^{\bullet +}$ and $dGuO^{\bullet +}$ were generated by CID of $[Cu^{II}(9MG)_3]^{\bullet 2+}$ and $[Cu^{II}(dGuo)_3]^{\bullet 2+}$, for which the ESI solution was prepared using 9MG and dGuo, respectively.

Radical cations were transported into the hexapole ion guide for collisional focusing and thermalization to 310 K, followed by mass selection in a quadrupole mass filter. Mass-selected reactant radical ions were injected into an octopole ion guide that passes a scattering cell containing the $^1O_2$ reactant. In addition to providing radio frequency potential that traps ions in the radial direction, the octopole was biased at a variable DC potential. The DC offset controlled the kinetic energy of reactant ions in the laboratory frame (E_{lab}) and thereby set the collision energy (E_{col}) between radical cations and $^1O_2$ in the center-of-mass frame using $E_{\mathrm{col}} = E_{\mathrm{lab}} \times m_{\mathrm{neutral}}/(m_{\mathrm{ion}} + m_{\mathrm{neutral}})$, where m_{ion} and m_{neutral} stand for masses of ionic and neutral reactants, respectively. After ion-molecule scattering, the product ions resulting from the reaction and the remaining reactant ions were collected by the octopole, passed into a second quadrupole mass filter for mass analysis, and counted by an electron multiplier detector. Reaction cross sections were calculated from the ratio of reactant/product ion intensities at each E_{col}, the pressure and the concentration of $^1O_2$ in the scattering cell, and the effective cell length. The scattering cell gas pressure (including $^1O_2$, $^3O_2$ and He) was maintained at 0.25 mτ. At this pressure, guanine radical cations had at most single collisions with oxygen molecule. It was reported that guanine radical cation does not present observable reaction with $^3O_2$.[68] The nonreactivity for the collisions of $9HG^{\bullet+}$, $9MG^{\bullet+}$, $dGuo^{\bullet+}$ and $Guo^{\bullet+}$ with $^3O_2$ was further verified in our control experiment conducted under the same conditions except that $^1O_2$ was replaced by $^3O_2$ gas.

The ion beam intensities were 3×10^5 cps for $9HG^{\bullet+}$, 8×10^5 cps for $9MG^{\bullet+}$, and 3×10^5 cps for $dGuo^{\bullet+}$ and $Guo^{\bullet+}$. Initial kinetic energy of the ion beam was set at 0.8 eV, with an energy spread controlled to be < 0.7 eV by collisional damping in the hexapole and reducing the radius of the ion beam at the exit of the first quadrupole. Monohydrated $9HG^{\bullet+}\cdot H_2O$ and $9MG^{\bullet+}\cdot H_2O$ were generated in a similar procedure, except that the sample solution was prepared in 2:1 methanol/water. The ion intensities were 2.4×10^4 and 4×10^4 cps for $9HG^{\bullet+}\cdot H_2O$ and $9MG^{\bullet+}\cdot H_2O$, respectively.

2.4 Electronic structure calculations

$9MG^{\bullet+}$ was utilized as a prototype for modeling guanosine radical cation reaction PES, of which the N9-methyl group mimics the nucleoside sugar moiety. As demonstrated in Scheme 1, $9MG^{\bullet+}$ has the same nucleobase conformation and the same spin density distribution (*i.e.*, an unpaired electron is delocalized among N3, C4, C5 and C8) as those of $dGuo^{\bullet+}$ and $Guo^{\bullet+}$.[65] It is thus reasonable to assume that the methyl-substitution at N9 has little effect on the relative enthalpies of oxidation intermediates, transition states (TSs) and products of guanosine,[52] as verified in our experiment. Geometries of reactants, intermediates, TSs and products were optimized using the ωB97XD[69] density functional theory (DFT) paired with the 6-31+G(d,p) basis set. This range-separated functional mitigates self-interaction errors and improves the orbital description of radical ions[70] than the B3LYP functional. The latter is known to introduce severe spin contamination in the $9MG^{\bullet+}$ reactant.[71]

The challenge in the calculation of PES for guanine radical cation with $^1O_2$ is that the system presents multi-configuration wavefunctions originating from the mixed open- and closed-shell character of $^1O_2$.[72] The spin-restricted DFT is unable to describe the static correlation arising from the two degenerate π^* antibonding orbitals and overestimates the $^1O_2$ excitation energy, whereas the broken-symmetry, spin-unrestricted DFT brings about spin contamination from the ground-state $^3O_2$. This problems exits not only in the $^1O_2$ reactant but also in the intermediates and TSs for $^1O_2$ addition to guanine.[43, 46-48] In our previous study of the $^1O_2$ reactions with protonated and deprotonated guanine ions,[46-48] spin contamination in the PES was corrected using Yamaguchi′s approximate spin-projection method,[73-74] in which the spin-projected total electronic energy of an open-shell singlet state was calculated as a weighted combination of broken-symmetry, spin-unrestricted singlet and triplet states. However, the approximate spin-projection was validated only for system containing singlet and triplet states.[43, 46-47, 73-74] The present system, on the other hand, is more complicated in that it mixes doublet and quartet states.

To obtain a reliable PES and therefore identify minimum energy reaction pathway(s), we have adopted a composite and more rigorous procedure in this work. DFT calculations at the ωB97XD/6-31+G(d,p) level were employed to map out all possible reaction pathways for the $^1O_2$-addition to $9MG^{\bullet+}$ and optimize all stationary points along reaction coordinates. All TSs were verified as first-order saddle points, and the vibrational mode associated with an imaginary frequency corresponds to the anticipated reaction pathway. Intrinsic reaction coordinate (IRC) calculation was carried out to substantiate reactant/product minima connected through each TS. Once reaction pathways were identified, electronic energies of all stationary structures and TSs were refined. First, two high-level, single-reference methods were applied for single-point energy calculations: the resolution-of-the-identity second-order Møller–Plesset perturbation theory (RI-MP2/aug-cc-pVQZ),[75-76] and the domain based local pair-natural orbital coupled-cluster single-, double- and perturbative triple-excitation method (DLPNO-CCSD(T)/aug-cc-pVTZ, where the inclusion of a perturbative correction for triple excitation may compensate for the deficiencies of a single-determinant reference).[77] Energies were further examined using the multi-reference complete active space self-consistent field method,[78-79] *i.e.*, CASSCF(9,7)/6-31+G(d,p) for

$9MG^{\bullet+}$, CASSCF(12,8)/6-31+G(d,p) for $^1O_2$, and CASSCF(21,15)/6-31+G(d,p) for other reaction species where the $\sigma_{O(2s)\text{-}O(2s)}$, $\sigma^*_{O(2s)\text{-}O(2s)}$, $\sigma_{O(2p)\text{-}O(2p)}$, $\pi_{\pm1}$, $\pi^*_{\pm1}$, and $\sigma^*_{O(2p)\text{-}O(2p)}$ orbitals of O_2 and the π orbitals of the guanine imidazole ring were included in the active space. Reaction enthalpy (ΔH) reported at each level of theory is based on the sum of the electronic energy calculated at the specified level and the 298 K thermal correction at ωB97XD/6-31+G(d,p) (including zero-point energy which was scaled by factor of 0.975[80]).

As we had expected, despite all single- and multi-reference methods predicted similar reaction coordinates, reaction potential energies were very sensitive to the theories. Particularly, the CASSCF calculations located most reaction intermediates and TSs above the reactants in energy, which was inconsistent with our experimental finding that the reaction is exothermic. The issue with the CASSCF calculations is that the electron correlation energy was treated in an unbalanced way and only that corresponds to the active orbitals (*i.e.*, static correlation) was considered. To take into account both static and dynamic correlations, we have proceeded to calculate the reaction PES using CASPT2(21,15)/6-31G(d,p),[81-82] *i.e.*, adding remaining dynamic correlation using second order perturbation theory with the CASSCF wave function as the reference. Since CASPT2 treats dynamic correlation effects perturbatively, it is less expensive than the multi-reference configuration interaction (MRCI) method[83] and allows for handling a large number of active orbitals for correlation.[81-82]

The ωB97XD/6-31+G(d,p) and CASSCF(21,15)/6-31+G(d,p) calculations were completed using Gaussian 09.[84] Electronic energies at the RI-MP2/aug-cc-pVQZ and DLPNO-CCSD(T)/aug-cc-pVTZ levels of theory were calculated with ORCA 4.[85] The CASPT2(21,15)/6-31G(d,p) calculations were carried out using MOLCAS 8,[86] for which the shift parameter for ionization potential-electron affinity (IPEA) was set to 0.25 a.u.[87-88]

3. Results and Discussion

3.1 Reaction products and cross sections

3.1.1 $^1O_2$ with $9HG^{\bullet+}$ and $9MG^{\bullet+}$. We first measured the ion-molecule scattering of $9HG^{\bullet+}$ and $9MG^{\bullet+}$

with $^1O_2$. For both systems, no products were detected over an E_{col} range from 0.05 to 1.0 eV except collision-induced fragment ions of the ionic reactants. A similar scenario was observed previously that no oxidation products were detected for the $^1O_2$ reactions with $[9HG + H]^+$, $[9MG + H]^+$, $[9HG - H]^-$ and $[9MG - H]^-$ ions.[44-45] The rationalization is that the nascent endoperoxide and/or exoperoxide adducts of guanine ions were energized by the reaction exothermicity and completely decayed back to the starting reactants during their time-of-flight within the mass spectrometer (~500 μs). In order to overcome this unfavorable reaction kinetics, we have employed an alternative method by using monohydrated reactant ions as the target for collisions with $^1O_2$. The idea was to enhance the energy relaxation of oxidation intermediates, *i.e.*, the reaction heat of formation, which would otherwise prompt the decomposition of an O_2-adduct, was used up mostly for eliminating a water ligand and the accompanying product kinetic energy release. By employing the water-evaporation cooling strategy, we have indeed observed the reaction products of $^1O_2$ with $9HG^{\bullet+}\cdot H_2O$ and $9MG^{\bullet+}\cdot H_2O$. Product ions were detected at $m/z = 183$ for $9HG^{\bullet+}\cdot H_2O + {}^1O_2$ and $m/z = 197$ for $9MG^{\bullet+}\cdot H_2O + {}^1O_2$, each of which corresponds to the liberation of a water ligand from an O_2-adduct of the hydrated reactant ion.

Figures 1a and b have shown the product ion cross sections for $9HG^{\bullet+}\cdot H_2O + {}^1O_2$ and $9MG^{\bullet+}\cdot H_2O + {}^1O_2$ as a function of E_{col} from 0.05 to 0.6 eV. Error bars were estimated on the basis of 4 sets of measurements. Insets present representative product ion mass spectra measured at $E_{col} = 0.05$ eV, where the product ion peaks were scaled by a factor of 100 for clarity. For both reaction systems, the product ion cross section decreases with increasing E_{col}, indicating that these reactions are exothermic and there are no activation barriers above the reactants. The fact that the reactions are able to eliminate a water ligand from the product complexes also indicates that the exothermicities of the oxidation reactions are more than the water binding energies of the products (0.7 eV, see below). This thermodynamic data will serve as experimental evidence to benchmark PES computation.

Reaction efficiency, estimated by $\sigma_{\text{reaction}}/\sigma_{\text{collision}}$ (where $\sigma_{\text{collision}}$ represents the ion-induced dipole capture cross section[89]), is 2% for $9HG^{\bullet+}\cdot H_2O$ and 1.4 % for $9MG^{\bullet+}\cdot H_2O$ at $E_{col} = 0.05$ eV, decreasing to

1.4% for $9HG^{\bullet+}\cdot H_2O$ and 1.3% for $9MG^{\bullet+}\cdot H_2O$ at 0.1 eV. Both reactions have become negligible above 0.6 eV. It appears that the 9-methyl substitution inhibits guanine oxidation.

3.1.2 $^1O_2$ with $dGuo^{\bullet+}$ and $Guo^{\bullet+}$. We have then measured the scattering of $dGuo^{\bullet+}$ and $Guo^{\bullet+}$ by $^1O_2$. In contrast to $9HG^{\bullet+}$ and $9MG^{\bullet+}$, the O_2-addition product ions were captured for both $dGuo^{\bullet+}$ and $Guo^{\bullet+}$ in their unhydrated states. This is probably due to the larger molecular size of $dGuo^{\bullet+}$ and $Guo^{\bullet+}$ than $9HG^{\bullet+}$ and $9MG^{\bullet+}$, and consequently more efficient intramolecular vibration redistribution (IVR) which helped deposit reaction heat of formation over vibrational modes without decomposing the products.

Figures 1c and d present product ion mass spectra and cross sections for $dGuo^{\bullet+}$ and $Guo^{\bullet+}$ over the E_{col} range of 0.05 – 0.5 eV. For both systems, the cross section generally increases with decreasing collision energy, but it dips at the lowest E_{col}. The dip is most likely artificial. To achieve an E_{col} below 0.1 eV in the center-of-mass frame, a retarding DC potential was applied to the octopole ion guide to deaccelerate the reactant ions. Due to the kinetic energy spread (~ 0.7 eV) of the ion beam, at the lowest E_{col} some reactant ions had nearly zero or backward axial velocity in the laboratory frame. This decreased the ion collection efficiency and consequently affected cross section measurement at the lowest E_{col}. The problem turned out to be more severe for $dGuo^{\bullet+}$ and $Guo^{\bullet+}$ than for $9HG^{\bullet+}$ and $9MG^{\bullet+}$.

Overall, the E_{col} dependence of product cross sections indicates that the $^1O_2$ reactions with $dGuo^{\bullet+}$ and $Guo^{\bullet+}$ are exothermic, analogous to those with $9HG^{\bullet+}$ and $9MG^{\bullet+}$. Taking into account the experimental uncertainties, the product cross sections for $dGuo^{\bullet+}$ and $Guo^{\bullet+}$ are comparable to each other. But they are approximately only half of those for $9HG^{\bullet+}\cdot H_2O$ and $9MG^{\bullet+}\cdot H_2O$. It is possible that, without additional energy relaxation such as water-evaporation cooling in a hydrated system, a fraction of nucleoside product ions have decomposed to the reactants before reaching the mass spectrometer detector. We have attempted to measure the $^1O_2$ reactions with $dGuo^{\bullet+}\cdot H_2O$ and $Guo^{\bullet+}\cdot H_2O$, but the beam intensities of monohydrated nucleoside radical cations were too low ($< 10^4$ cps) to allow for meaningful measurements.

3.2 PES for the $^1O_2$ addition to $9MG^{\bullet+}$

3.2.1 Overview of reaction pathways and products. PES for $9MG^{\bullet+}$ with $^1O_2$ was explored first using the ωB97XD/6-31+G(d,p) method. The one-dimensional PES of the resulting pathways is depicted in Figure 2, including ChemDraw structures of all reaction intermediates, TSs and products. Cartesian coordinates for these species are provided in the Supporting Information. Four $^1O_2$-addition mechanisms were identified, and all of them are initiated at a reactant-like, π-stacked precursor complex:

1) Concerted Diels-Alder cycloaddition of O_2 across the imidazole C5-C8 bond. The reaction is mediated by TS58 and leads to the formation of a 5,8-endoperoxide ($[5,8\text{-OO-9MG}]^{\bullet+}$), as illustrated by the red line in Figure 2a. Along the reaction coordinate, the unpaired electron diffuses from the guanine moiety to the O_2 orbital as verified by the DFT-calculated spin density distribution and the CASSCF-calculated singly occupied molecular orbital (SOMO), but the positive charge remains at the guanine imidazole ring. Therefore, spin and charge are separating in the reaction. To emphasize that the spin density is delocalized throughout the system, the superscript •+ is applied over the whole reaction structure that is bracketed together. We have explored the possibility of forming a 4,8-endoperoxide, as the latter structure is known to form in the $^1O_2$ cycloaddition to neutral guanine and guanosine.[30, 43] However, a $[4,8\text{-OO-9MG}]^{\bullet+}$-like geometry converged to either $[5,8\text{-OO-9MG}]^{\bullet+}$ or $[8\text{-OO-9MG}]^{\bullet+}$.

2) C8-terminal addition of O_2 (shown by black lines in Figure 2a). There are two possible routes which lead to the same product structure but with the *anti*- and *syn*-configurations, respectively, with respect to the imidazole ring. $^1O_2$ may attack at the C8 terminal via TS8a to produce *anti*-$[8\text{-OO-9MG}]^{\bullet+}$, followed by interconversion to *syn*-$[8\text{-OO-9MG}]^{\bullet+}$ via a rotation barrier TS8b. Alternatively, *syn*-$[8\text{-OO-9MG}]^{\bullet+}$ may be formed directly from the reactants by crossing over TS8c. Compared to that of *anti*-$[8\text{-OO-9MG}]^{\bullet+}$, the formation of *syn*-$[8\text{-OO-9MG}]^{\bullet+}$ has a lower activation barrier and higher exothermicity and thus is more kinetically facile and thermodynamically favorable. *syn*-$[8\text{-OO-9MG}]^{\bullet+}$ may serve as an intermediate for a ring-closure reaction to $[5,8\text{-OO-9MG}]^{\bullet+}$, *i.e.*, the nucleophilic attack of the distal O atom of the peroxo group at the C5 atom via TS8d. In this sense, cycloaddition proceeds stepwise. The subsequent barrier TS8d for ring closure is significantly higher than the initial barrier TS8a (or TS8c) for $^1O_2$ addition, but is comparable to the barrier TS58 for concerted cycloaddition. The unpaired electron is

delocalized among the imidazole ring and O_2 in TS8a, TS8c and TS8d, and completely shifts to the $\pi^*_{O\text{-}O}$ orbital in TS8b and *anti*- and *syn*-[8-OO-9MG]$^{\bullet+}$. As a result, the spin-charge separation increases continuously along the reaction pathways.

3) C4- and C5-terminal addition of O_2 (shown by green and blue lines in Figure 2b). The two pathways follow a similar pattern. The C4-addition produces an *anti*-[4-OO-9MG]$^{\bullet+}$ via TS4a and a *syn*-[4-OO-9MG]$^{\bullet+}$ via TS4c. The two rotamers of [4-OO-9MG]$^{\bullet+}$ may interconvert via TS4b, and *syn*-[4-OO-9MG]$^{\bullet+}$ may convert to *syn*-[5-OO-9MG]$^{\bullet+}$ via TS4d. Similarly, the C5-addition produces *anti*- and *syn*-[5-OO-9MG]$^{\bullet+}$. In both C4- and C5-peroxides, the barriers for rotation are small and the *syn*-conformers may be slightly more stable, analogous to the pair of *anti*- and *syn*-C8-peroxides. *syn*-[5-OO-9MG]$^{\bullet+}$ may follow a stepwise cycloaddition to form [5,8-OO-9MG]$^{\bullet+}$ via TS5d or a dioxetane [4,5-OO-9MG]$^{\bullet+}$ via TS5e. An interesting finding is that the formation of 4,5-[OO-9MG]$^{\bullet+}$ could be initiated only at [5-OO-9MG]$^{\bullet+}$ but not at [4-OO-9MG]$^{\bullet+}$.

The spin-charge separation was also observed along the C4- and C5-addition pathways. While the positive charge is localized at the imidazole ring, the spin density is shared among the imidazole and the $\pi^*_{O\text{-}O}$ orbital in TS4a (mostly on O_2), TS4c (mostly on O_2), TS4d (mostly on O_2), TS5a, TS5c, TS5d, TS5e and [4,5-OO-9MG]$^{\bullet+}$, and completely relocated to the $\pi^*_{O\text{-}O}$ orbital in TS4b, TS5b, *anti*- and *syn*-[4-OO-9MG]$^{\bullet+}$, and *anti*- and *syn*-[5-OO-9MG]$^{\bullet+}$.

3.2.2 Reaction energies at the single-reference levels and T1 diagnostic. Table 1 compares reaction enthalpies calculated at the ωB97XD/6-31+G(d,p), RI-MP2/aug-cc-pVQZ and DLPNO-CCSD(T)/aug-cc-pVTZ levels of theory. Reactions PESs constructed at the RI-MP2 and DLPNO-CCSD(T) levels are presented in the Supporting Information. On the one hand, the three different theories have predicted qualitatively similar reaction coordinates and pathways. Particularly, all peroxide-formation pathways are exothermic with no activation barriers above the reactants, except the TS8a calculated at RI-MP2. For each peroxide, the *anti*- and *syn*-conformers are comparable in terms of reaction activation barrier and product heat of formation, with the *syn*-conformer being slightly more favored. Of the three peroxides,

$[8\text{-OO-9MG}]^{\bullet+}$ has the lowest energy, followed by $[5\text{-OO-9MG}]^{\bullet+}$ and then $[4\text{-OO-9MG}]^{\bullet+}$. On the other hand, the three theories have given rise to sizable differences in the reaction energies. For the formation of $[5,8\text{-OO-9MG}]^{\bullet+}$, the ωB97XD and DLPNO-CCSD(T)-calculated barriers are 0.2 – 0.35 eV above the reactants, whereas the RI-MP2 barrier is 0.26 eV below the reactants. The formation of $[4,5\text{-OO-9MG}]^{\bullet+}$ was calculated to be exothermic at ωB97XD but becomes endothermic at RI-MP2 and DLPNO-CCSD (T). Large deviations (from 0.79 eV up to 1.13 eV) were also observed in the reaction enthalpies of the precursor complex as well as TS8a, TS8c, TS5a, TS5c and TS5d. As the reaction approaches the C8-, C5- and C4- peroxides and 5,8-endoperxoide, the energies at the three levels are getting close and the differences decrease to ≤ 0.24 eV.

As aforementioned, single Slater-determinant wavefunctions may not be reliable in describing the open-shell electronic structures of $^1O_2$ and its complexes with guanine radical cation. To quantitatively assess whether the calculated structures are dominated by single-determinant wavefunctions, T1 diagnostic[90-91] was performed at the CCSD(T)/aug-cc-pVTZ level of theory for all of the structures. For a closed-shell system, a T1 diagnostic larger than 0.02 implies that the system is not well described by a single-reference method. There exist other important configurations that are needed as references in a treatment of nondynamic electron correlation.[90] However, it is less clear what exactly constitutes a suspiciously large T1 for an open-shell system.[91-93] In the present work, the T1 diagnostic was used to mainly compare various species on the reaction PES and explore how the multi-reference character evolves along each reaction pathway.

The T1 diagnostic results of the coupled-cluster wavefunctions are collected in Table 1. Among the stationary structures, the precursor complex and $[4,5\text{-OO-9MG}]^{\bullet+}$ have T1 exceeding 0.02. Besides, the TSs that lead to the formation of endoperoxides from peroxides (*i.e.*, TS5d leading from *syn*-$[5\text{-OO-9MG}]^{\bullet+}$ to $[5,8\text{-OO-9MG}]^{\bullet+}$, TS5e from *syn*-$[5\text{-OO-9MG}]^{\bullet+}$ to $[4,5\text{-OO-9MG}]^{\bullet+}$ and TS8d from *syn*-$[8\text{-OO-9MG}]^{\bullet+}$ to $[5,8\text{-OO-9MG}]^{\bullet+}$) and the TS4d for the interconversion between *syn*-$[4\text{-OO-9MG}]^{\bullet+}$ and *syn*-$[5\text{-OO-9MG}]^{\bullet+}$ have T1 larger than 0.02. Coincidently, these structures have the spin density delocalized among the imidazole ring and the O_2 orbital. This demonstrates a strong correlation between spin density distribution and T1 diagnostic.

3.2.3 Experimental benchmark for reaction thermodynamics. Since the reaction product of $9MG^{\bullet+}\cdot H_2O$ corresponds to the O_2 addition accompanying with elimination of a water ligand, the heat release from $^1O_2$ oxidation must be larger than the water ligand elimination energy (or product ion hydration energy). Only in this case, the water molecule can be liberated barrierlessly following the O_2 addition.

Scheme 2 illustrates the structures of monohydrated $9MG^{\bullet+}$ and its peroxide products. Table 2 compares the water ligand elimination energies ($\Delta H_{\text{water eli}}$) of these peroxides at the single-reference levels. Assuming that spin contamination in the peroxides is similar in the absence and the presence of a water ligand, its effect tends to largely cancel off on water ligand elimination. As a result, the ωB97XD, RI-MP2 and DLPNO-CCSD(T) methods have shown a good agreement (within 0.1 eV) in the $\Delta H_{\text{water eli}}$ value for each peroxide. On average, the water ligand elimination energy is 0.7 eV. On the basis of this experimental evidence, all of the reaction pathways which have an exothermicity over 0.7 eV and an activation barrier below the reactants could be detected in our experiment. The *anti*- and *syn*-conformers of $[5\text{-OO-9MG}]^{\bullet+}$ and $[8\text{-OO-9MG}]^{\bullet+}$ have the exothermicity larger than 0.7 eV and therefore may be considered as probable products. On the other hand, *anti*- and *syn*-$[4\text{-OO-9MG}]^{\bullet+}$, $[5,8\text{-OO-9MG}]^{\bullet+}$ and $[4,5\text{-OO-9MG}]^{\bullet+}$ either have a formation exothermicity much less than 0.7 eV or involve an activation barrier above the reactants, and therefore may not be captured in the experiment. Of course, the calculations of reaction enthalpies have suffered spin contamination at the single-reference levels; as such, the analysis for experimental products needs to be validated at the multi-reference levels as discussed below.

3.2.4 Reaction energies at the multi-reference levels and importance of dynamic electron correlation. Finally, reaction PESs were explored at the CASSCF(21,15)/6-31+G(d,p) and CASPT2(21,15)/6-31G(d,p) levels of theory. Their reaction energies are appended to Table 1, and their

PESs are compared in Figure 3. The CASSCF and CASPT2-calculated reaction pathways have followed the same reaction coordinates as those predicted by the single-reference calculations. In addition, there is a good correlation between the spin density distributions determined at ωB97XD and the SOMO orbitals mapped at CASSCF and CASPT2. However, the CASSCF calculations have significantly increased reaction energies. According to the CASSCF results, the *anti*- and *syn*-[8-OO-9MG]$^{\bullet+}$ are the only two exothermic product channels (reaction ΔH is -0.28 and -0.33 eV, respectively), but both bear a significant activation barrier (0.94 and 0.82 eV, respectively). These energies are clearly overestimated; otherwise, there would have been no products detected in our experiment. This indicates that CASSCF is problematic in treating the reaction of $^1O_2$ with radicals. A similar problem was reported for the reaction of $^1O_2$ with neutral guanine molecule by Schlegel and coworkers,[43] in which the addition barriers and the energies of the reaction intermediates were overestimated by CASSCF.

As rationalized above, a major problem of CASSCF is that it includes primarily nondynamic electron correlation. To improve the agreement with experiment, second order perturbation theory corrections are required to account for dynamic correlation. For example, a composite CASPT2/DFT approach (*i.e.*, single-point CASPT2 energy calculations of open-shell geometries optimized at DFT) was found to produce correct PESs for the $^1O_2$ reactions with alkenes[72] and 1,3-cyclohexadiene, [43,94] and the predicted barrier energies were consistent with the experimental data. A more related work was reported by Marchetti and Karsili,[95] in which CASPT2 was used to explore the $^1O_2$ addition to neutral guanine and histidine. Inspired by these works, we have refined the PES at CASPT2(21,15)/6-31G(d,p). As a calibration of the CASPT2 energy, we calculated the singlet-triplet energy gap of O_2 using CASPT2(12,8)/6-31G(d,p). CASPT2 has predicted an excitation energy of 1.04 eV for $^1O_2$, close to the experimental value of 0.98 eV.[62] The superior performance of CASPT2 over CASSCF can be comprehended in detail in Figure 3, wherein the differences between the CASSCF and CASPT2 energies are indicated. It appears that dynamic correlations are the most significant in TS58 (0.90 eV), TS8a (1.44 eV), TS8c (1.66 eV) and TS4a (1.38 eV), where the numbers in the parentheses represent the energy corrections by CASPT2. The energy correction for dynamic correlation becomes less prominent as the reaction approaches the end products.

Note that, for most reaction species, the CASPT2 energy is 0.5 – 0.7 eV higher than the ωB97XD energy. This energy difference closely matches the amount of excitation energy that was overestimated (0.7 eV) for the $^1O_2$ reactant by the spin restricted ωB97XD. The exceptions are some *syn*-O_2 addition barriers, for which the CASPT2 and ωB97XD energies differ either less than 0.4 eV (*i.e.*, TS8c) or more than 1.9 eV (*i.e.*, TS5c). The RI-MP2 method also overstabilized reaction species than CASPT2 by a variable range from 0.2 to 1.2 eV, except TS8a, TS8c, TS5a and TS5d for which the energies raised at RI-MP2. Similarly, the DLPNO-CCSD(T) method overstabilized species by a range of 0.2 – 1.8 eV, except that the precursor complex became less stable by 0.52 eV with respect to CASPT2.

On the basis of the CASPT2 PES, the most probable experimental product channel corresponds to reactants → precursor → TS8c → *syn*-$[8\text{-OO-9MG}]^{\bullet+}$ (the barrier TS8c has shifted to an energy below the product, thus the reaction becomes barrierless), followed by reactants → precursor → TS8a → *anti*-$[8\text{-OO-9MG}]^{\bullet+}$ → TS8b → *syn*-$[8\text{-OO-9MG}]^{\bullet+}$. Both *anti*- and *syn*-$[8\text{-OO-9MG}]^{\bullet+}$ products have formation enthalpies above (or close to) 0.7 eV and no activation barriers above the reactants. The product exothermicity of *anti*- and *syn*-$[5\text{-OO-9MG}]^{\bullet+}$ is only ~0.1 eV less than the water ligand elimination energy, so the formation of theses product ions is possible at E_{col} above 0.1 eV. The CASPT2 PES also suggests that 5,8-cycloaddition, 4,5-addition and C4-terminal addition are endothermic and thus could be ruled out in the experiment.

3.2.5 Comparison with the $^1O_2$ oxidation of $[9MG + H]^+$ and $[9MG – H]^–$. We have previously reported experimental and computational studies of the $^1O_2$ reactions with $[9MG + H]^+\cdot H_2O$ (protonated at the N7 position) and $[9MG – H]^-\cdot H_2O$ (deprotonated at the N1 position).[45] The $^1O_2$ oxidation of $[9MG + H]^+$ is dominated by a concerted 5,8-cycloaddition, and the $[5,8\text{-OO-9HG} + H]^+$ endoperoxide appeared as the only product. The same type of reaction becomes the least probable for $9MG^{\bullet+}$. A concerted cycloaddition does not occur for $[9MG – H]^–$. Instead, the $^1O_2$ addition to $[9MG – H]^–$ is mediated by a stepwise addition starting with the formation of a [8-OO-9MG – H]$^-$ peroxide, which subsequently evolves to a [4,8-OO-9MG – H]$^-$ endoperoxide. Besides, no [5,8-OO-9MG – H]$^-$ endoperoxide could be formed in the reaction. The distinctively different oxidation pathways for 9MG$^{\bullet+}$, [9MG + H]$^+$ and [9MG – H]$^-$ have reinforced the premise that different ionization states lead to different guanine oxidation mechanisms.

Similar to that of guanine radical cation, the N9-methyl substitution in the protonated and deprotonated guanine ions decreases their reaction efficiencies with $^1O_2$, *i.e.*, the reaction efficiency is 2.4% for [9HG + H]$^+\cdot H_2O$ and [9HG – H]$^-\cdot H_2O$,[44] decreasing to 1.3 – 1.7% for [9MG + H]$^+\cdot H_2O$ and [9MG – H]$^-\cdot H_2O$,[45] all of which were measured at 0.1 eV.

4. Conclusions

The present work is aimed to assess the chemistry of guanine radical cation with electronically excited $^1O_2$ for the first time. The reactions for $^1O_2$ with 9HG$^{\bullet+}$, 9MG$^{\bullet+}$, dGuo$^{\bullet+}$ and Guo$^{\bullet+}$ were measured in the gas phase using guided-ion-beam scattering mass spectrometry. All of the reactions produced peroxide product ions, with the reaction cross sections in the order of 9HG$^{\bullet+}$ > 9MG$^{\bullet+}$ > dGuo$^{\bullet+}$ ≈ Guo$^{\bullet+}$. These reactions were all found to be exothermic with no reaction barriers above the starting reactants, and the product exothermicities are above 0.7 eV. 9MG$^{\bullet+}$ was chosen as a model compound to explore the reaction PES for the $^1O_2$ oxidation of guanine radical cation computationally. The ωB97XD, RI-MP2, DLPNO-CCSD(T), CASSCF and CASPT2 levels of theory have been each applied to the PES calculations. The different levels of theory have all predicted four reaction routes: a concerted 5,8-cycloaddition to the formation of an endoperoxide [5,8-OO-9MG]$^{\bullet+}$, and C8-, C4-, and C5-terminal addition pathways to the formation of various peroxides ([8-OO-9MG]$^{\bullet+}$, [4-OO-9MG]$^{\bullet+}$ and [5-OO-9MG]$^{\bullet+}$) and then to a dioxetane [4,5-OO-9MG]$^{\bullet+}$. However, due to the multireference characters in the mixed open-and closed-shell $^1O_2$ and in the open-shell $^1O_2$-adducts and transition states, the single-determinant reference calculations have suffered spin contamination, while the CASSCF was struggling for the lack of a treatment of dynamic electron correlation. A successfully approach was to use CASPT2 which couples complete active space with the corrections for dynamic correlation by second order perturbation theory. The CASPT2-predicted reaction PES is consistent with the experimental measurement of reaction activation barrier and product enthalpy. Guided by experimental and computational evidence, it was predicted that the most probable reaction pathway for the oxidation of guanine radical cation corresponds to the formation of 8-peroxide. The formation of 5-peroxide may be possible in the experiment, but the formation of 4-peroxide, 5,8-endoperoxide or 4,5-dioxetane were ruled out on the basis of unfavorable reaction barrier and/or reaction endothermicity. Finally, the distinctively different $^1O_2$ reaction pathways of guanine radical cation compared to those of protonated and deprotonated guanine ions reported before have emphasized the dependence of nucleobase oxidation mechanism on ionization states.

Acknowledgements

This work was supported by National Science Foundation (Grant No. CHE 1856362). Y. Sun acknowledges CUNY Mina Rees Dissertation Fellowship. The authors are grateful to Prof. Jing Xie and Mr. Mengkai Liu (Beijing Institute of Technology) for guiding CASPT2 calculations. This work is dedicated to Prof. Cheuk-Yiu Ng. J. Liu would like to thank Prof. Cheuk-Yiu Ng for inspiration and guidance in ion spectroscopy and dynamics.

Supporting Information

PESs at RI-MP2/aug-cc-pVQZ and DLPNO-CCSD(T)/aug-cc-pVTZ, and Cartesian Coordinates for the calculated structures

References

(1) Steenken, S.; Jovanovic, S. V., How Easily Oxidizable Is DNA? One-Electron Reduction Potentials of Adenosine and Guanosine Radicals in Aqueous Solution. *J. Am. Chem. Soc.* **1997,** *119*, 617-618.

(2) Burrows, C. J.; Muller, J. G., Oxidative Nucleobase Modifications Leading to Strand Scission. *Chem. Rev.* **1998,** *98*, 1109-1151.

(3) Zhou, J.; Kostko, O.; Nicolas, C.; Tang, X.; Belau, L.; de Vries, M. S.; Ahmed, M., Experimental Observation of Guanine Tautomers with VUV Photoionization. *J. Phys. Chem. A* **2009,** *113*, 4829-4832.

(4) Schwell, M.; Hochlaf, M., Photoionization Spectroscopy of Nucleobases and Analogues in the Gas Phase Using Synchrotron Radiation as Excitation Light Source. *Top. Curr. Chem.* **2015,** *355*, 155-208.

(5) Candeias, L. P.; Steenken, S., Structure and Acid-Base Properties of One-Electron-Oxidized Deoxyguanosine, Guanosine, and 1-Methylguanosine. *J. Am. Chem. Soc.* **1989,** *111*, 1094-9.

(6) Steenken, S., Purine Bases, Nucleosides, and Nucleotides: Aqueous Solution Redox Chemistry and Transformation Reactions of Their Radical Cations and e^- and OH Adducts. *Chem. Rev.* **1989,** *89*, 503-20.

(7) Candeias, L. P.; Steenken, S., Ionization of Purine Nucleosides and Nucleotides and Their Components by 193-nm Laser Photolysis in Aqueous Solution: Model Studies for Oxidative Damage of DNA. *J. Am. Chem. Soc.* **1992,** *114*, 699-704.

(8) Saito, I.; Nakamura, T.; Nakatani, K., Mapping of Highest Occupied Molecular Orbitals of Duplex DNA by Cobalt-Mediated Guanine Oxidation. *J. Am. Chem. Soc.* **2000,** *122*, 3001-3006.

(9) Stemp, E. D. A.; Barton, J. K., Electron Transfer between Metal Complexes Bound to DNA: Is DNA a Wire? *Met. Ions Biol. Syst.* **1996,** *33*, 325-365.

(10) Thorp, H. H., Cutting out the Middleman: DNA Biosensors Based on Electrochemical Oxidation. *Trends Biotechnol.* **1998,** *16*, 117-121.

(11) Ribaut, C.; Bordeau, G.; Perio, P.; Reybier, K.; Sartor, V.; Reynes, O.; Fabre, P.-L.; Chouini-Lalanne, N., EPR Spectroelectrochemical Investigation of Guanine Radical Formation and Environment Effects. *J. Phys. Chem. B* **2014,** *118*, 2360-2365.

(12) Kasai, H.; Yamaizumi, Z.; Berger, M.; Cadet, J., Photosensitized Formation of 7,8-Dihydro-8-oxo-2'-deoxyguanosine (8-Hydroxy-2'-deoxyguanosine) in DNA by Riboflavin: A Non Singlet Oxygen-Mediated Reaction. *J. Am. Chem. Soc.* **1992,** *114*, 9692-4.

(13) Hall, J. P.; Poynton, F. E.; Keane, P. M.; Gurung, S. P.; Brazier, J. A.; Cardin, D. J.; Winter, G.; Gunnlaugsson, T.; Sazanovich, I. V.; Towrie, M., et al., Monitoring One-Electron Photo-Oxidation of Guanine in DNA Crystals Using Ultrafast Infrared Spectroscopy. *Nat. Chem.* **2015,** *7*, 961-967.

(14) Caruso, T.; Carotenuto, M.; Vasca, E.; Peluso, A., Direct Experimental Observation of the Effect of the Base Pairing on the Oxidation Potential of Guanine. *J. Am. Chem. Soc.* **2005,** *127*, 15040-15041.

(15) Crespo-Hernández, C. E.; Close, D. M.; Gorb, L.; Leszczynski, J., Determination of Redox Potentials for the Watson-Crick Base Pairs, DNA Nucleosides, and Relevant Nucleoside Analogs. *J. Phys. Chem. B* **2007,** *111*, 5386-5395.

(16) Hutter, M.; Clark, T., On the Enhanced Stability of the Guanine-Cytosine Base-Pair Radical Cation. *J. Am. Chem. Soc.* **1996,** *118*, 7574-7577.

(17) Jaeger, H. M.; Schaefer, H. F., III, Characterizing Radiation-Induced Oxidation of DNA by Way of the Monohydrated Guanine-Cytosine Radical Cation. *J. Phys. Chem. B* **2009,** *113*, 8142-8148.

(18) Lewis, F. D.; Liu, X.; Liu, J.; Miller, S. E.; Hayes, R. T.; Wasielewski, M. R., Direct Measurement of Hole Transport Dynamics in DNA. *Nature* **2000,** *406*, 51-53.

(19) Cadet, J.; Berger, M.; Buchko, G. W.; Joshi, P. C.; Raoul, S.; Ravanat, J.-L., 2,2-Diamino-4-[(3,5-di-*O*-acetyl-2-deoxy-*β*-D-erythro-pentofuranosyl)amino]-5-(2H)-oxazolone: A Novel and Predominant Radical Oxidation Product of 3',5'-di-*O*-acetyl-2'-deoxyguanosine. *J. Am. Chem. Soc.* **1994,** *116*, 7403-4.

(20) Cadet, J.; Douki, T.; Ravanat, J.-L., Oxidatively Generated Damage to the Guanine Moiety of DNA: Mechanistic Aspects and Formation in Cells. *Acc. Chem. Res.* **2008,** *41*, 1075-1083.

(21) Neeley, W. L.; Essigmann, J. M., Mechanisms of Formation, Genotoxicity, and Mutation of Guanine Oxidation Products. *Chem. Res. Toxicol.* **2006,** *19*, 491-505.

(22) Fleming, A. M.; Burrows, C. J., Formation and Processing of DNA Damage Substrates for the hNEIL Enzymes. *Free Radic. Biol. Med.* **2017,** *107*, 35-52.

(23) Boiteux, S.; Radicella, J. P., Base Excision Repair of 8-Hydroxyguanine Protects DNA from Endogenous Oxidative Stress. *Biochimie* **1999,** *81*, 59-67.

(24) Ogilby, P. R., Singlet Oxygen: There Is Indeed Something New under the Sun. *Chem. Soc. Rev.* **2010,** *39*, 3181-3209.

(25) *Singlet Oxygen: Applications in Biosciences and Nanosciences, Volume 1. [In: Compr. Ser. Photochem. Photobiol. Sci., 2016; 13]*. Nonell, S.; Flors, C., Eds,; RSC: Cambridge, 2016; p 472 pp.

(26) Ravanat, J.-L.; Di Mascio, P.; Martinez, G. R.; Medeiros, M. H. G.; Cadet, J., Singlet Oxygen Induces Oxidation of Cellular DNA. *J. Biol. Chem.* **2000,** *275*, 40601-40604.

(27) Cadet, J.; Douki, T.; Pouget, J.-P.; Ravanat, J.-L., Singlet Oxygen DNA Damage Products: Formation and Measurement. *Methods Enzymol.* **2000,** *319*, 143-153.

(28) Cadet, J.; Ravanat, J.-L.; Martinez, G. R.; Medeiros, M. H. G.; Di Mascio, P., Singlet Oxygen Oxidation of Isolated and Cellular DNA: Product Formation and Mechanistic Insights. *Photochem. Photobiol.* **2006,** *82*, 1219-1225.

(29) Cadet, J.; Douki, T.; Ravanat, J.-L., Oxidatively Generated Base Damage to Cellular DNA. *Free Radic. Biol. Med.* **2010,** *49*, 9-21.

(30) Sheu, C.; Foote, C. S., Endoperoxide Formation in a Guanosine Derivative. *J. Am. Chem. Soc.* **1993,** *115*, 10446-10447.

(31) Ravanat, J.-L.; Douki, T.; Cadet, J., Direct and Indirect Effects of UV Radiation on DNA and Its Components. *J. Photochem. Photobiol., B* **2001,** *63*, 88-102.

(32) Ravanat, J.-L.; Saint-Pierre, C.; Di Mascio, P.; Martinez, G. R.; Medeiros, M. H. G.; Cadet, J., Damage to Isolated DNA Mediated by Singlet Oxygen. *Helv. Chim. Acta* **2001,** *84*, 3702-3709.

(33) Niles, J. C.; Wishnok, J. S.; Tannenbaum, S. R., Spiroiminodihydantoin Is the Major Product of the 8-Oxo-7,8-dihydroguanosine Reaction with Peroxynitrite in the Presence of Thiols and Guanosine Photooxidation by Methylene Blue. *Org. Lett.* **2001,** *3*, 963-966.

(34) Kang, P.; Foote, C. S., Formation of Transient Intermediates in Low-Temperature Photosensitized Oxidation of an 8-^{13}C-Guanosine Derivative. *J. Am. Chem. Soc.* **2002,** *124*, 4865-4873.

(35) Ye, Y.; Muller, J. G.; Luo, W.; Mayne, C. L.; Shallop, A. J.; Jones, R. A.; Burrows, C. J., Formation of ^{13}C-, ^{15}N-, and ^{18}O-Labeled Guanidinohydantoin from Guanosine Oxidation with Singlet Oxygen. Implications for Structure and Mechanism. *J. Am. Chem. Soc.* **2003,** *125*, 13926-13927.

(36) Ravanat, J.-L.; Martinez, G. R.; Medeiros, M. H. G.; Di Mascio, P.; Cadet, J., Mechanistic Aspects of the Oxidation of DNA Constituents Mediated by Singlet Molecular Oxygen. *Arch. Biochem. Biophys.* **2004,** *423*, 23-30.

(37) McCallum, J. E. B.; Kuniyoshi, C. Y.; Foote, C. S., Characterization of 5-Hydroxy-8-oxo-7,8-dihydroguanosine in the Photosensitized Oxidation of 8-Oxo-7,8-dihydroguanosine and Its Rearrangement to Spiroiminodihydantoin. *J. Am. Chem. Soc.* **2004,** *126*, 16777-16782.

(38) Iesce, M. R.; Cermola, F.; Temussi, F., Photooxygenation of Heterocycles. *Curr. Org. Chem.* **2005,** *9*, 109-139.

(39) Ravanat, J.-L.; Martinez, G. R.; Medeiros, M. H. G.; Di Mascio, P.; Cadet, J., Singlet Oxygen Oxidation of 2'-Deoxyguanosine. Formation and Mechanistic Insights. *Tetrahedron* **2006,** *62*, 10709-10715.

(40) Gimisis, T.; Cismas, C., Isolation, Characterization, and Independent Synthesis of Guanine Oxidation Products. *Eur. J. Org. Chem.* **2006,** *2006*, 1351-1378.

(41) Dumont, E.; Gruber, R.; Bignon, E.; Morell, C.; Moreau, Y.; Monari, A.; Ravanat, J.-L., Probing the Reactivity of Singlet Oxygen with Purines. *Nucleic Acids Res.* **2016,** *44*, 56-62.

(42) Dumont, E.; Gruber, R.; Bignon, E.; Morell, C.; Aranda, J.; Ravanat, J.-L.; Tunon, I., Singlet Oxygen Attack on Guanine: Reactivity and Structural Signature within the B-DNA Helix. *Chem. Eur. J.* **2016,** *22*, 12358-12362.

(43) Thapa, B.; Munk, B. H.; Burrows, C. J.; Schlegel, H. B., Computational Study of Oxidation of Guanine by Singlet Oxygen ($^1\Delta_g$) and Formation of Guanine:Lysine Cross-Links. *Chem. - Eur. J.* **2017,** *23*, 5804-5813.

(44) Lu, W.; Liu, J., Capturing Transient Endoperoxide in the Singlet Oxygen Oxidation of Guanine. *Chem. Eur. J.* **2016,** *22*, 3127-3138.

(45) Lu, W.; Teng, H.; Liu, J., How Protonation and Deprotonation of 9-Methylguanine Alter Its Singlet O_2 Addition Path: About the Initial Stage of Guanine Nucleoside Oxidation. *Phys. Chem. Chem. Phys.* **2016,** *18*, 15223-15234.

(46) Lu, W.; Sun, Y.; Tsai, M.; Zhou, W.; Liu, J., Singlet O_2 Oxidation of Deprotonated Guanine-Cytosine Base Pair and Its Entangling with Intra-Base-Pair Proton Transfer. *ChemPhysChem* **2018,** *19*, 2645-2654.

(47) Lu, W.; Sun, Y.; Zhou, W.; Liu, J., Ph-Dependent Singlet O_2 Oxidation Kinetics of Guanine and 9-Methylguanine: An Online Mass Spectrometry and Spectroscopy Study Combined with Theoretical Exploration. *J. Phys. Chem. B* **2018,** *122*, 40-53.

(48) Sun, Y.; Tsai, M.; Zhou, W.; Lu, W.; Liu, J., Reaction Kinetics, Product Branching, and Potential Energy Surfaces of $^1O_2$-Induced 9-Methylguanine–Lysine Cross-Linking: A Combined Mass Spectrometry, Spectroscopy, and Computational Study. *J. Phys. Chem. B* **2019,** *123*, 10410-10423.

(49) Bruner, S. D.; Norman, D. P. G.; Verdine, G. L., Structural Basis for Recognition and Repair of the Endogenous Mutagen 8-Oxoguanine in DNA. *Nature* **2000,** *403*, 859-866.

(50) Marnett, L. J.; Burcham, P. C., Endogenous DNA Adducts: Potential and Paradox. *Chem. Res. Toxicol.* **1993,** *6*, 771-85.

(51) Palumbo, G., Photodynamic Therapy and Cancer: A Brief Sightseeing Tour. *Expert Opin. Drug Delivery* **2007,** *4*, 131-148.

(52) Munk, B. H.; Burrows, C. J.; Schlegel, H. B., An Exploration of Mechanisms for the Transformation of 8-Oxoguanine to Guanidinohydantoin and Spiroiminodihydantoin by Density Functional Theory. *J. Am. Chem. Soc.* **2008,** *130*, 5245-5256.

(53) Ye, Y.; Munk, B. H.; Muller, J. G.; Cogbill, A.; Burrows, C. J.; Schlegel, H. B., Mechanistic Aspects of the Formation of Guanidinohydantoin from Spiroiminodihydantoin under Acidic Conditions. *Chem. Res. Toxicol.* **2009,** *22*, 526-535.

(54) Colasanti, A.; Kisslinger, A.; Quarto, M.; Riccio, P., Combined Effects of Radiotherapy and Photodynamic Therapy on an *in Vitro* Human Prostate Model. *Acta Biochim. Pol.* **2004,** *51*, 1039-1046.

(55) Postiglione, I.; Chiaviello, A.; Palumbo, G., Enhancing Photodynamic Therapy Efficacy by Combination Therapy: Dated, Current and Oncoming Strategies. *Cancers* **2011,** *3*, 2597-2629.

(56) Lo, V. C. K.; Akens, M. K.; Moore, S.; Yee, A. J. M.; Wilson, B. C.; Whyne, C. M., Beyond Radiation Therapy: Photodynamic Therapy Maintains Structural Integrity of Irradiated Healthy and Metastatically Involved Vertebrae in a Pre-Clinical *in Vivo* Model. *Breast Cancer Res. Treat.* **2012,** *135*, 391-401.

(57) Kobayashi, K.; Tagawa, S., Direct Observation of Guanine Radical Cation Deprotonation in Duplex DNA Using Pulse Radiolysis. *J. Am. Chem. Soc.* **2003,** *125*, 10213-10218.

(58) Kobayashi, K.; Yamagami, R.; Tagawa, S., Effect of Base Sequence and Deprotonation of Guanine Cation Radical in DNA. *J. Phys. Chem. B* **2008,** *112*, 10752-10757.

(59) Sun, Y.; Moe, M. M.; Liu, J., Mass Spectrometry and Computational Study of Collision-Induced Dissociation of 9-Methylguanine-1-Methylcytosine Base-Pair Radical Cation: Intra-Base-Pair Proton Transfer and Hydrogen Transfer, Non-Statistical Dissociation, and Reaction with a Water Ligand. *Phys. Chem. Chem. Phys.* **2020,** *20*, 14875-14888.

(60) Midey, A.; Dotan, I.; Viggiano, A. A., Temperature Dependences for the Reactions of O^- and O_2^- with $O_2(a^1\Delta_g)$ from 200 to 700 K. *J. Phys. Chem. A* **2008,** *112*, 3040-3045.

(61) Fang, Y.; Liu, F.; Bennett, A.; Ara, S.; Liu, J., Experimental and Trajectory Study on Reaction of Protonated Methionine with Electronically Excited Singlet Molecular Oxygen ($a^1\Delta_g$): Reaction Dynamics and Collision Energy Effects. *J. Phys. Chem. B* **2011,** *115*, 2671-2682.

(62) Lafferty, W. J.; Solodov, A. M.; Lugez, C. L.; Fraser, G. T., Rotational Line Strengths and Self-Pressure-Broadening Coefficients for the 1.27 Mm, $a^1\Delta_g$-$X^3\Sigma_g^-$, ν = 0-0 Band of O_2. *Appl. Opt.* **1998,** *37*, 2264-2270.

(63) Liu, F.; Fang, Y.; Chen, Y.; Liu, J., Reactions of Deprotonated Tyrosine and Tryptophan with Electronically Excited Singlet Molecular Oxygen ($a^1\Delta_g$): A Guided-Ion-Beam Scattering, Statistical Modeling, and Trajectory Study. *J. Phys. Chem. B* **2012,** *116*, 6369-6379.

(64) Fang, Y.; Liu, J., Reaction of Protonated Tyrosine with Electronically Excited Singlet Molecular Oxygen ($a^1\Delta_g$): An Experimental and Trajectory Study. *J. Phys. Chem. A* **2009,** *113*, 11250-11261.

(65) Sun, Y.; Zhou, W.; Moe, M. M.; Liu, J., Reactions of Water with Radical Cations of Guanine, 9-Methylguanine, 2'-Deoxyguanosine and Guanosine: Keto-Enol Isomerization, C8-Hydroxylation, and Effects of N9-Substitution. *Phys. Chem. Chem. Phys.* **2018,** *20*, 27510-27522.

(66) Cheng, P.; Bohme, D. K., Gas-Phase Formation of Radical Cations of Monomers and Dimers of Guanosine by Collision-Induced Dissociation of Cu(II)-Guanosine Complexes. *J. Phys. Chem. B* **2007,** *111*, 11075-11082.

(67) Feketeová, L.; Yuriev, E.; Orbell, J. D.; Khairallah, G. N.; O'Hair, R. A. J., Gas-Phase Formation and Reactions of Radical Cations of Guanosine, Deoxyguanosine and Their Homodimers and Heterodimers. *Int. J. Mass Spectrom.* **2011,** *304*, 74-82.

(68) Al-Sheikhly, M., The Reactivity of Adenyl and Guanyl Radicals Towards Oxygen. *Radiat. Phys. Chem.* **1994,** *44*, 297-301.

(69) Chai, J.-D.; Head-Gordon, M., Long-Range Corrected Hybrid Density Functionals with Damped Atom–Atom Dispersion Corrections. *Phys. Chem. Chem. Phys.* **2008,** *10*, 6615-6620.

(70) Kumar, A.; Sevilla, M. D., Proton Transfer Induced Somo-to-Homo Level Switching in One-Electron Oxidized A-T and G-C Base Pairs: A Density Functional Theory Study. *J. Phys. Chem. B* **2014,** *118*, 5453-5458.

(71) Reynisson, J.; Steenken, S., DFT Calculations on the Electrophilic Reaction with Water of the Guanine and Adenine Radical Cations. A Model for the Situation in DNA. *Phys. Chem. Chem. Phys.* **2002,** *4*, 527-532.

(72) Maranzana, A.; Ghigo, G.; Tonachini, G., Diradical and Peroxirane Pathways in the [π2 + π2] Cycloaddition Reactions of $^1\Delta_g$ Dioxygen with Ethene, Methyl Vinyl Ether, and Butadiene: A Density Functional and Multireference Perturbation Theory Study. *J. Am. Chem. Soc.* **2000,** *122*, 1414-1423.

(73) Saito, T.; Nishihara, S.; Kataoka, Y.; Nakanishi, Y.; Matsui, T.; Kitagawa, Y.; Kawakami, T.; Okumura, M.; Yamaguchi, K., Transition State Optimization Based on Approximate Spin-Projection (AP) Method. *Chem. Phys. Lett.* **2009,** *483*, 168-171.

(74) Saito, T.; Nishihara, S.; Kataoka, Y.; Nakanishi, Y.; Kitagawa, Y.; Kawakami, T.; Yamanaka, S.; Okumura, M.; Yamaguchi, K., Reinvestigation of the Reaction of Ethylene and Singlet Oxygen by the Approximate Spin Projection Method. Comparison with Multireference Coupled-Cluster Calculations. *J. Phys. Chem. A* **2010,** *114*, 7967-7974.

(75) Weigend, F.; Haser, M.; Patzelt, H.; Ahlrichs, R., RI-MP2: Optimized Auxiliary Basis Sets and Demonstration of Efficiency. *Chem. Phys. Lett.* **1998,** *294*, 143-152.

(76) Jurecka, P.; Nachtigall, P.; Hobza, P., RI-MP2 Calculations with Extended Basis Sets – a Promising Tool for Study of H-Bonded and Stacked DNA Base Pairs. *Phys. Chem. Chem. Phys.* **2001,** *3*, 4578-4582.

(77) Liakos, D. G.; Sparta, M.; Kesharwani, M. K.; Martin, J. M. L.; Neese, F., Exploring the Accuracy Limits of Local Pair Natural Orbital Coupled-Cluster Theory. *J. Chem. Theory Comput.* **2015,** *11*, 1525-1539.

(78) Roos, B. O.; Taylor, P. R.; Sigbahn, P. E. M., A Complete Active Space Scf Method (CASSCF) Using a Density Matrix Formulated Super-CI Approach. *Chem. Phys.* **1980,** *48*, 157-73.

(79) Olsen, J.; Roos, B. O.; Jøgensen, P.; Jensen, H. J. A., Determinant Based Configuration Interaction Algorithms for Complete and Restricted Configuration Interaction Spaces. *J. Chem. Phys.* **1988,** *89*, 2185-92.

(80) Alecu, I. M.; Zheng, J.; Zhao, Y.; Truhlar, D. G., Computational Thermochemistry: Scale Factor Databases and Scale Factors for Vibrational Frequencies Obtained from Electronic Model Chemistries. *J. Chem. Theory Comput.* **2010,** *6*, 2872-2887.

(81) Andersson, K.; Malmqvist, P. A.; Roos, B. O., Second-Order Perturbation Theory with a Complete Active Space Self-Consistent Field Reference Function. *J. Chem. Phys.* **1992,** *96*, 1218-26.

(82) Abe, M.; Gopakmar, G.; Nakajima, T.; Hirao, K., Relativistic Multireference Perturbation Theory: Complete Active-Space Second-Order Perturbation Theory (CASPT2) with the Four-Component Dirac Hamiltonian. In *Radiation Induced Molecular Phenomena in Nucleic Acids*, Shukla, K.; K., M.; Leszczynski, J., Eds. Springer: Netherlands, 2008; pp 157-177.

(83) Buenker, R. J.; Peyerimhoff, S. D., Individualized Configuration Selection in CI Calculations with Subsequent Energy Extrapolation. *Theor. Chim. Acta* **1974,** *35*, 33-58.

(84) Frisch, M. J.; Trucks, G. W.; Schlegel, H. B.; Scuseria, G. E.; Robb, M. A.; Cheeseman, J. R.; Scalmani, G.; Barone, V.; Mennucci, B.; Petersson, G. A., et al. *Gaussian 09, Rev. D.01*, Gaussian, Inc: Wallingford, CT, 2013.

(85) Neese, F., Software Update: The Orca Program System, Version 4.0. *WIREs Comput Mol Sci* **2018,** *8*, e1327.

(86) Aquilante, F.; Autschbach, J.; Carlson, R. K.; Chibotaru, L. F.; Delcey, M. G.; De Vico, L.; Fdez. Galvan, I.; Ferre, N.; Frutos, L. M.; Gagliardi, L., et al., Molcas 8: New Capabilities for Multiconfigurational Quantum Chemical Calculations across the Periodic Table. *J. Comput. Chem.* **2016,** *37*, 506-541.

(87) Roca-Sanjuán, D.; Rubio, M.; Merchán, M.; Serrano-Andrés, L., Ab Initio Determination of the Ionization Potentials of DNA and RNA Nucleobases. *J. Chem. Phys.* **2006,** *125*, 084302.

(88) Ghigo, G.; Roos, B. O.; Malmqvist, P.-A., A Modified Definition of the Zeroth-Order Hamiltonian in Multiconfigurational Perturbation Theory (CASPT2). *Chem. Phys. Lett.* **2004,** *396*, 142-149.

(89) Troe, J., Statistical Adiabatic Channel Model of Ion-Neutral Dipole Capture Rate Constants. *Chem. Phys. Lett.* **1985,** *122*, 425-430.

(90) Lee, T. J.; Taylor, P. R., A Diagnostic for Determining the Quality of Single-Reference Electron Correlation Methods. *Int. J. Quantum Chem., Quantum Chem. Symp.* **1989,** *36*, 199-207.

(91) Jayatilaka, D.; Lee, T. J., Open-Shell, Coupled-Cluster Theory. *J. Chem. Phys.* **1993,** *98*, 9734-47.

(92) Rienstra-Kiracofe, J. C.; Allen, W. D.; Schaefer, H. F., III, The $C_2H_5 + O_2$ Reaction Mechanism: High-Level Ab Initio Characterizations. *J. Phys. Chem. A* **2000,** *104*.

(93) Lee, T. J., Comparison of the T1 and D1 Diagnostics for Electronic Structure Theory: A New Definition for the Open-Shell D1 Diagnostic. *Chem. Phys. Lett.* **2003,** *372*, 362-367.

(94) Sevin, F.; McKee, M. L., Reactions of 1,3-Cyclohexadiene with Singlet Oxygen. A Theoretical Study. *J. Am. Chem. Soc.* **2001,** *123*, 4591-4600.

(95) Marchetti, B.; Karsili, T. N. V., An Exploration of the Reactivity of Singlet Oxygen with Biomolecular Constituents. *Chem. Commun.* **2016,** *52*, 10996-10999.

Table 1. Relative enthalpies (eV, 298 K) of reaction species calculated at the single- and multi-reference levels of theory and their T1 diagnostic

species	ωB97XD/ 6-31+G(d,p)	RI-MP2/ aug-cc-pVQZ [a]	DLPNO-CCSD(T)/ aug-cc-pVTZ [a]	CASSCF(21,15)/ 6-31+G(d,p) [a,b]	CASPT2(21,15) 6-31G(d,p) [a,c]	T1 diagnostic
$9MG^{\bullet +} + {}^{1}O_2$	0.0	0.0	0.0	0.0	0.0	0.019 ($9MG^{\bullet +}$) 0.015 (${}^{1}O_2$)
precursor	-1.75	-1.38	-0.64	-0.95	-1.16	0.027
TS58	0.20	-0.26	0.35	1.61	0.71	0.018
[5,8-OO-9MG]$^{\bullet +}$	-0.57	-0.72	-0.48	0.45	0.21	0.016
TS8a	-0.93	0.20	-0.66	0.94	-0.50	0.019
anti-[8-OO-9MG]$^{\bullet +}$	-1.33	-1.28	-1.15	-0.28	-0.58	0.019
TS8b	-1.17	-1.13	-0.98	-0.08	-0.54	0.019
TS8c	-1.20	-0.23	-1.03	0.82	-0.84	0.020
syn-[8OO-9MG]$^{\bullet +}$	-1.40	-1.35	-1.23	-0.33	-0.78	0.019
TS8d	0.25	0.24	0.38	1.47	0.70	0.023
TS4a	-0.50	-0.45	-0.27	1.44	0.06	0.020
anti-[4OO-9MG]$^{\bullet +}$	-0.48	-0.46	-0.29	0.70	0.13	0.020
TS4b	-0.39	-0.40	-0.24	0.70	0.20	0.019
TS4c	-0.49	-0.47	-0.30	0.89	0.19	0.020
syn-[4-OO-9MG]$^{\bullet +}$	-0.49	-0.48	-0.35	0.61	0.12	0.020
TS4d	0.07	0.09	0.29	1.38	0.61	0.022
TS5a	-1.02	-0.21	-0.84	0.03	-0.71	0.020
anti-[5-OO-9MG]$^{\bullet +}$	-1.16	-1.10	-0.96	0.02	-0.59	0.020
TS5b	-1.09	-1.04	-0.90	0.19	-0.53	0.019
TS5c	-1.07	-0.28	-0.89	0.95	0.88	0.020
syn-[5-OO-9MG]$^{\bullet +}$	-1.16	-1.11	-0.97	-0.04	-0.58	0.020
TS5d	0.16	1.19	0.71	1.49	0.82	0.048
TS5e	-0.16	0.12	0.14	1.16	0.49	0.025
[4,5-OO-9MG]$^{\bullet +}$	-0.18	0.38	0.08	1.24	0.59	0.023

a) using ωB97XD/6-31+G(d,p)-calculated geometries and thermal corrections.

b) CASSCF(9,7)/6-31+G(d,p) was used for $9MG^{\bullet +}$ and CASSCF(12,8)/6-31+G(d,p) for ${}^{1}O_2$.

c) CASPT2(9,7)/6-31G(d,p) was used for $9MG^{\bullet +}$ and CASPT2(12,8)/6-31G(d,p) for ${}^{1}O_2$.

Table 2. Comparison of water ligand elimination energy ($\Delta H_{\text{water eli}}$, eV) for various monohydrated peroxide products at the single-reference levels of theory

species	ωB97XD/6-31+G(d,p)	RI-MP2/aug-cc-pVQZ [a]	DLPNO-CCSD(T)/aug-cc-pVTZ [a]
anti-[8-OO-9MG]$^{\bullet+}\cdot H_2O$	0.79	0.71	0.69
syn-[8-OO-9MG]$^{\bullet+}\cdot H_2O$	0.79	0.70	0.69
anti-[4-OO-9MG]$^{\bullet+}\cdot H_2O$	0.73	0.64	0.63
syn-[4-OO-9MG]$^{\bullet+}\cdot H_2O$	0.72	0.64	0.63
anti-[5-OO-9MG]$^{\bullet+}\cdot H_2O$	0.79	0.71	0.70
syn-[5-OO-9MG]$^{\bullet+}\cdot H_2O$	0.79	0.70	0.70

a) using ωB97XD/6-31+G(d,p)-calculated geometries and thermal corrections.

Scheme 1. The lowest-energy structures of $9HG^{\bullet+}$, $9MG^{\bullet+}$, $dGuo^{\bullet+}$ and $Guo^{\bullet+}$ optimized at the ωB97XD/6-31+G(d,p) level of theory, with atomic numbering schemes. Spin densities are represented by contour plots and charge densities are indicated in numbers. Their Cartesian coordinates are available in the Supporting Information.

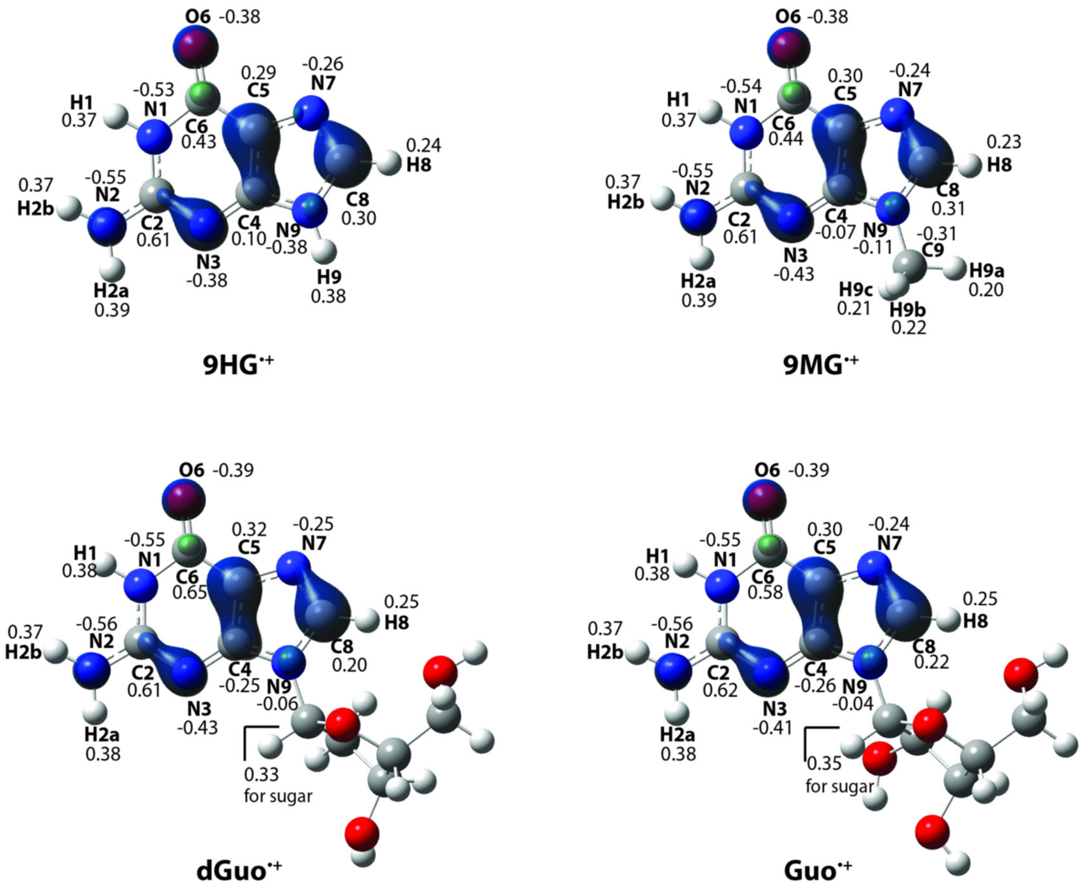

$9HG^{\bullet+}$ $9MG^{\bullet+}$

$dGuo^{\bullet+}$ $Guo^{\bullet+}$

Scheme 2. The lowest-energy structures of monohydrated 9MG$^{\bullet+}$ and its peroxide products optimized at the ωB97XD/6-31+G(d,p) level of theory. Their Cartesian coordinates are available in the Supporting Information.

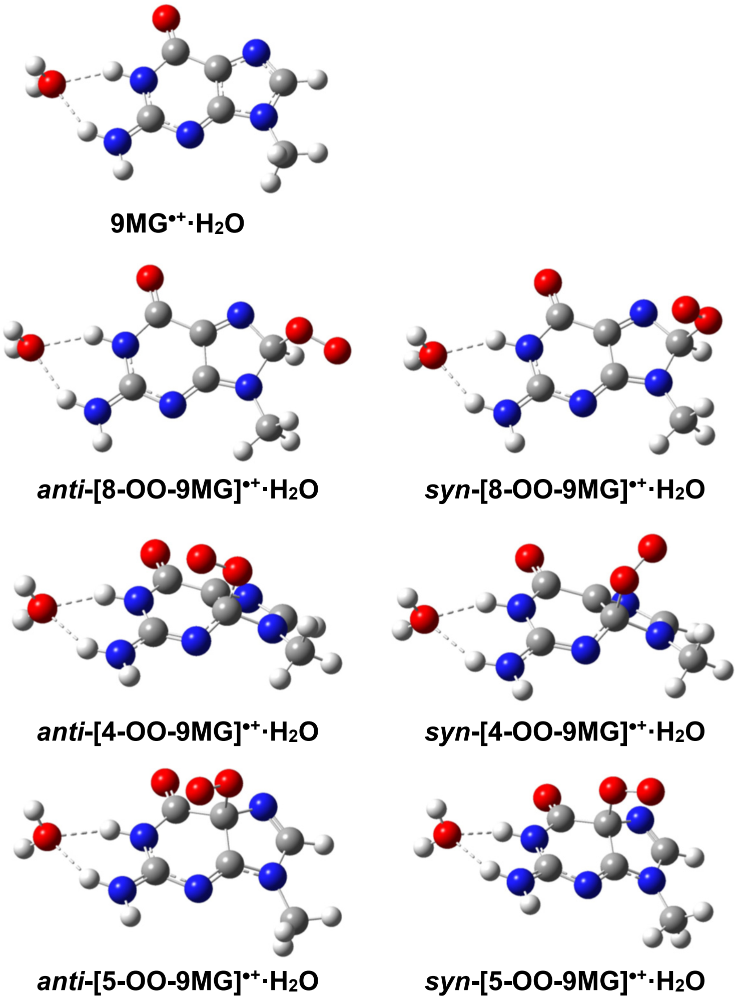

$9MG^{\bullet+}\cdot H_2O$

***anti*-$[8\text{-}OO\text{-}9MG]^{\bullet+}\cdot H_2O$**

***syn*-$[8\text{-}OO\text{-}9MG]^{\bullet+}\cdot H_2O$**

***anti*-$[4\text{-}OO\text{-}9MG]^{\bullet+}\cdot H_2O$**

***syn*-$[4\text{-}OO\text{-}9MG]^{\bullet+}\cdot H_2O$**

***anti*-$[5\text{-}OO\text{-}9MG]^{\bullet+}\cdot H_2O$**

***syn*-$[5\text{-}OO\text{-}9MG]^{\bullet+}\cdot H_2O$**

Figure Caption

Fig. 1 Product cross sections for the $^1O_2$ reactions with (a) $9HG^{\bullet+}\cdot H_2O$, (b) $9MG^{\bullet+}\cdot H_2O$, (c) $dGuo^{\bullet+}$ and (d) $Guo^{\bullet+}$. Insets show product ion mass spectra.

Fig. 2 Reaction pathways for the $^1O_2$ addition to $9MG^{\bullet+}$. Structures and reaction enthalpies were calculated at the ωB97XD/6-31+G(d,p) level of theory, including thermal corrections at 298 K. For TSs, vibrational mode corresponding to the imaginary frequency is indicated by displacement vectors in the ChemDraw structures. Cartesian coordinates for the calculated structures are available in the Supporting Information.

Fig. 3 Comparison of multi-configuration PES for the $^1O_2$ addition to $9MG^{\bullet+}$ calculated at the CASSCF(21e, 15o)/6-31+G(d,p) and CASPT2(21e, 15o)/6-31G(d,p) levels of the theory, using the ωB97XD/6-31+G(d,p)-optimized geometries. Reaction enthalpies were calculated at 298 K including thermal corrections.

Fig. 1

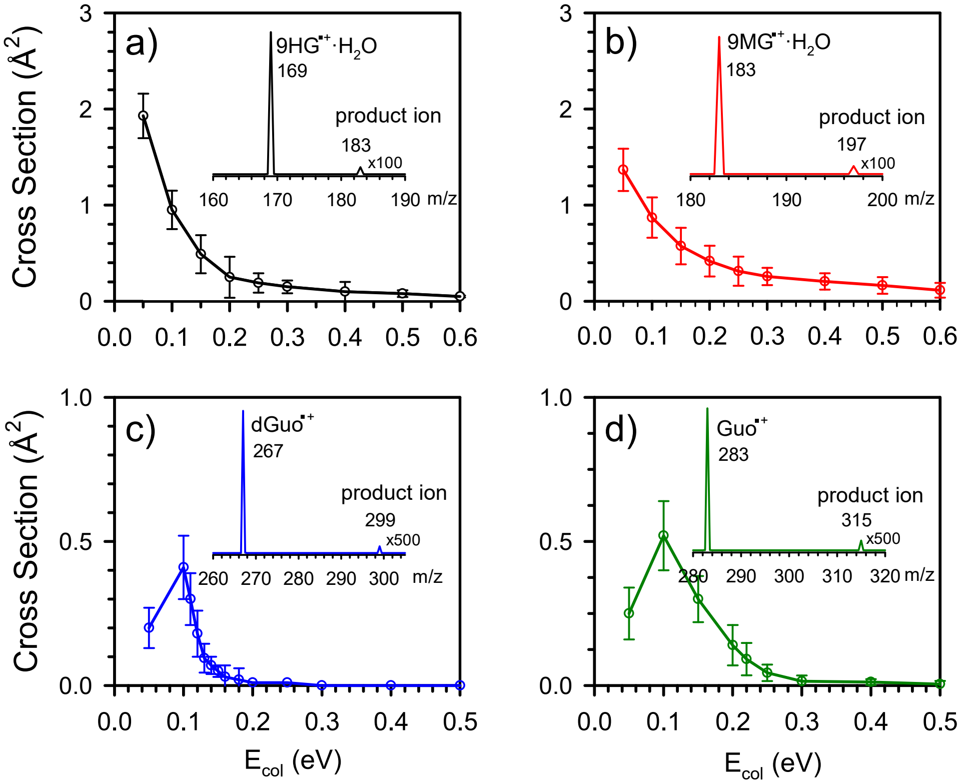
a)
9HG•+·H2O
169
product ion
183
x100
160
170
180
190
m/z
b)
9MG•+·H2O
183
product ion
197
x100
180
190
200
m/z
c)
dGuo•+
267
product ion
299
x500
260
270
280
290
300
m/z
d)
Guo•+
283
product ion
315
x500
280
290
300
310
320
m/z
Cross Section (Å2)
0
1
2
3
0.0
0.5
1.0
0.0
0.1
0.2
0.3
0.4
0.5
0.6
Ecol (eV)

Fig. 2

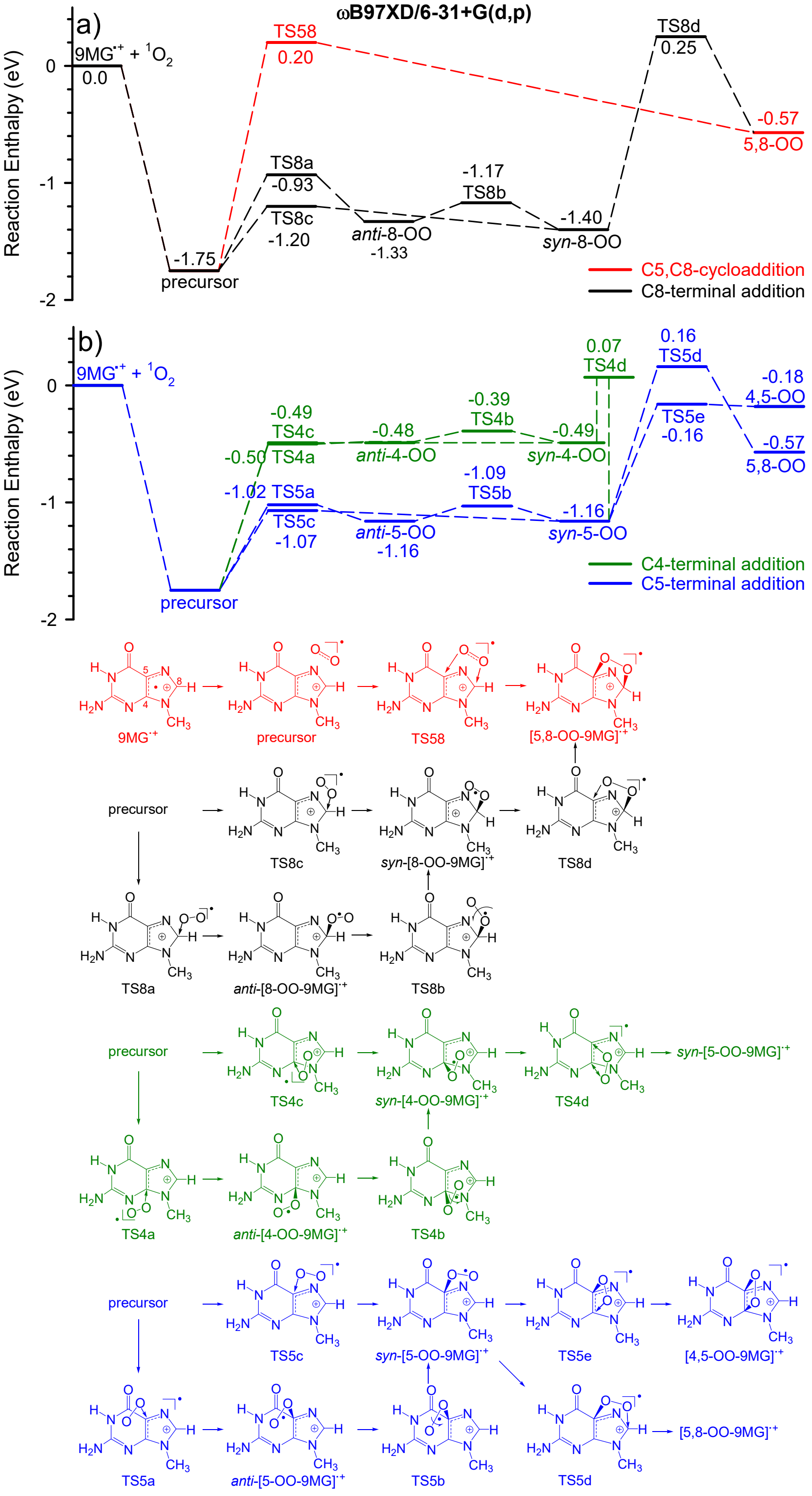
ωB97XD/6-31+G(d,p)
a)
Reaction Enthalpy (eV)
0
-1
-2
9MG•+ + 1O2
0.0
TS58
0.20
TS8d
0.25
-0.57
5,8-OO
TS8a
-0.93
-1.17
TS8b
-1.40
syn-8-OO
TS8c
-1.20
anti-8-OO
-1.33
-1.75
precursor
C5,C8-cycloaddition
C8-terminal addition
b)
Reaction Enthalpy (eV)
0
-1
-2
9MG•+ + 1O2
0.07
TS4d
0.16
TS5d
-0.18
4,5-OO
-0.49
TS4c
-0.48
anti-4-OO
-0.39
TS4b
-0.49
syn-4-OO
-0.50
TS4a
TS5e
-0.16
-0.57
5,8-OO
-1.02
TS5a
-1.09
TS5b
-1.16
syn-5-OO
TS5c
-1.07
anti-5-OO
-1.16
precursor
C4-terminal addition
C5-terminal addition
9MG•+
precursor
TS58
[5,8-OO-9MG]•+
precursor
TS8c
syn-[8-OO-9MG]•+
TS8d
TS8a
anti-[8-OO-9MG]•+
TS8b
precursor
TS4c
syn-[4-OO-9MG]•+
TS4d
syn-[5-OO-9MG]•+
TS4a
anti-[4-OO-9MG]•+
TS4b
precursor
TS5c
syn-[5-OO-9MG]•+
TS5e
[4,5-OO-9MG]•+
TS5a
anti-[5-OO-9MG]•+
TS5b
TS5d
[5,8-OO-9MG]•+

Fig. 3

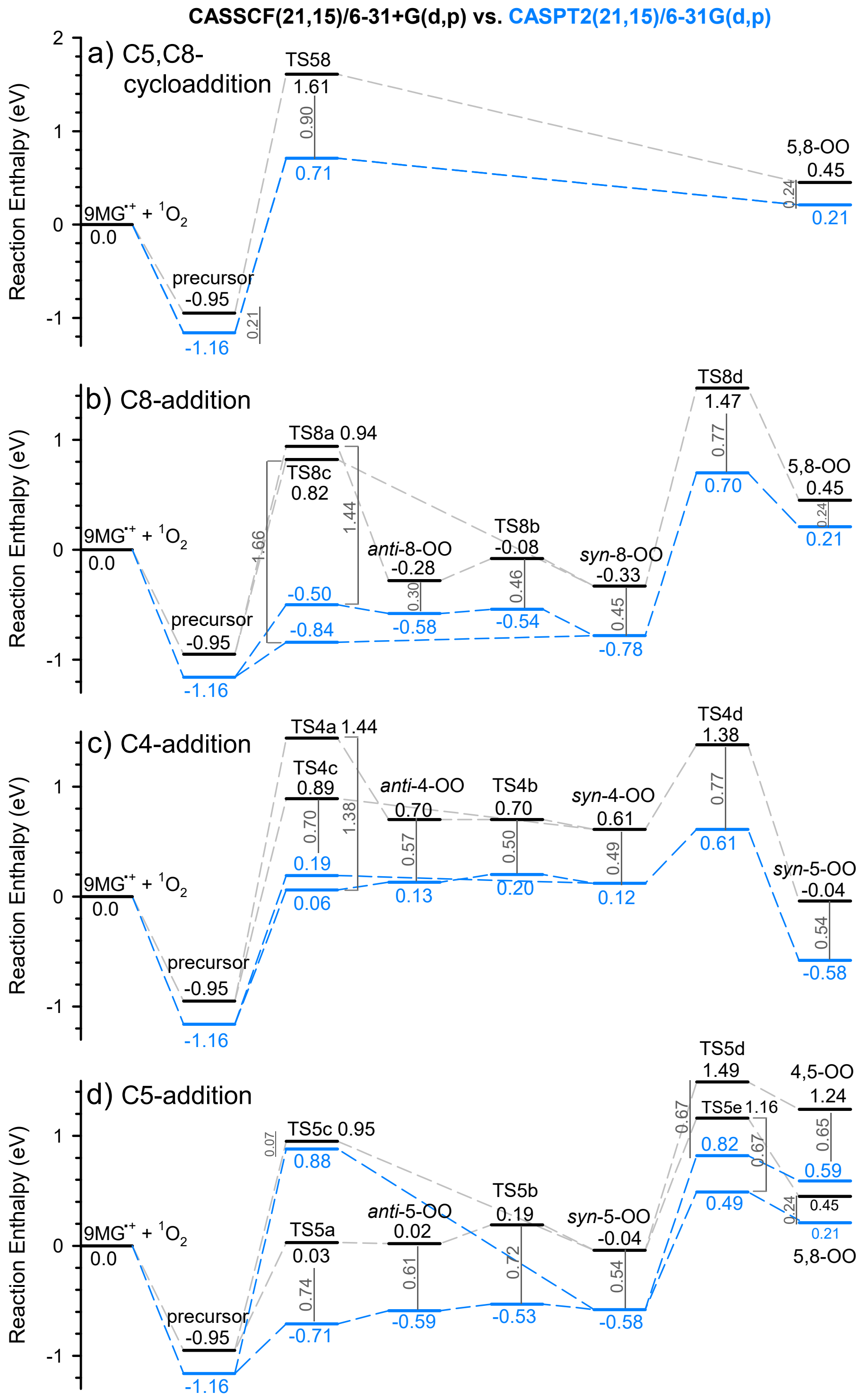
CASSCF(21,15)/6-31+G(d,p) vs. CASPT2(21,15)/6-31G(d,p)
Reaction Enthalpy (eV)
2
1
0
-1
a) C5,C8-cycloaddition
$9MG^{\cdot+}$ + $^1O_2$
0.0
precursor
-0.95
-1.16
0.21
TS58
1.61
0.90
0.71
5,8-OO
0.45
0.24
0.21
b) C8-addition
$9MG^{\cdot+}$ + $^1O_2$
0.0
precursor
-0.95
-1.16
1.66
TS8a 0.94
TS8c
0.82
1.44
-0.50
-0.84
anti-8-OO
-0.28
0.30
-0.58
TS8b
-0.08
0.46
-0.54
syn-8-OO
-0.33
0.45
-0.78
TS8d
1.47
0.77
0.70
5,8-OO
0.45
0.24
0.21
c) C4-addition
$9MG^{\cdot+}$ + $^1O_2$
0.0
precursor
-0.95
-1.16
TS4a 1.44
TS4c
0.89
0.70
1.38
0.19
0.06
anti-4-OO
0.70
0.57
0.13
TS4b
0.70
0.50
0.20
syn-4-OO
0.61
0.49
0.12
TS4d
1.38
0.77
0.61
syn-5-OO
-0.04
0.54
-0.58
d) C5-addition
$9MG^{\cdot+}$ + $^1O_2$
0.0
precursor
-0.95
-1.16
0.07
TS5c 0.95
0.88
TS5a
0.03
0.74
-0.71
anti-5-OO
0.02
0.61
-0.59
TS5b
0.19
0.72
-0.53
syn-5-OO
-0.04
0.54
-0.58
0.67
TS5d
1.49
TS5e 1.16
0.82
0.67
0.49
4,5-OO
1.24
0.65
0.59
0.45
0.24
0.21
5,8-OO

TOC Graphics